Supraglacial lakes on the Larsen B Ice Shelf, Antarctica, and at Paakitsoq, W. Greenland: a comparative study

Alison F. Banwell[1,2], Martamaria Caballero[3,1], Neil S. Arnold[2], Neil F. Glasser[4], L. Mac Cathles[1], Douglas R. MacAyeal[1]

1. *Department of Geophysical Sciences, University of Chicago, Chicago, IL, USA*
2. *Scott Polar Research Institute, University of Cambridge, Lensfield Road, Cambridge, CB2 1ER, UK*
3. *Centro Mario Molina Chile, Av. Providencia 2133, Oficina 603, Santiago, Chile.*
4. *Centre for Glaciology, Institute of Geography and Earth Sciences, Aberystwyth University, Ceredigion SY23 3DB, UK*

ABSTRACT

Supraglacial meltwater lakes trigger ice-shelf break-up and modulate seasonal ice-sheet flow, and are thus agents by which warming is transmitted to the Antarctic and Greenland ice sheets. To characterize supraglacial lake variability we perform a comparative analysis of lake geometry and depth in two distinct regions, one on the pre-collapse (2002) Larsen B Ice Shelf, and the other in the ablation zone of Paakitsoq, a land-terminating region of the Greenland Ice Sheet. Compared to Paakitsoq, lakes on the Larsen B Ice Shelf cover a greater proportion of surface area (5.3% vs. 1%), but are shallower and more uniform in area. Other aspects of lake geometry, such as eccentricity, degree of convexity (solidity) and orientation, are relatively similar between the two regions. We attribute the notable difference in lake density and depth between ice-shelf and grounded ice to the fact that ice shelves have flatter surfaces and less distinct drainage basins. Ice shelves also possess more stimuli to small-scale, localized surface elevation variability due to the various structural features that yield small variations in thickness and which float at different levels by Archimedes' principle.

1. INTRODUCTION

Supraglacial lake dynamics have become an increasingly important factor in ice sheet response to climate change because lakes have been implicated in ice shelf disintegration (e.g., Scambos and others, 2003) and influenced grounded ice sheet flow through their impact on subglacial hydrology. When lakes on ice sheets suddenly drain (e.g., Das and others, 2008; Doyle and others, 2013; Tedesco and others, 2013), the subglacial drainage system receives a pulse of water that, in turn, contributes to both temporary and longer-term changes in ice velocity (Bartholomew and others, 2011; Hoffman and others, 2011; Banwell and others, 2013; Joughin and others, 2013). Within the ablation zone of the Greenland Ice Sheet (GrIS), supraglacial lakes form in surface depressions controlled by the interplay between bedrock topography and ice flow (Echelmeyer and others, 1991; Sergienko, 2013; Darnell and others, 2013). This means that processes unrelated to climate change (i.e., bedrock characteristics and ice flow physics) determine the areal distribution, maximum depth and volume of the lakes.

In contrast, lakes on floating ice shelves do not depend on ice/bedrock interaction to define their location, geometry and volume. Instead, lakes on ice shelves inhabit various surface depressions that arise from a variety of processes, e.g., basal crevassing (McGrath and others, 2012), grounding zone flow-stripe development (Glasser and Gudmundsson, 2012), and intermittent suture-zone voids (Glasser and others, 2009). Lakes on ice shelves are also products of the viscoelastic flexure of the ice, and can represent a surface load that can suddenly change when fractures develop through the ice shelf causing lake drainage through hydrofracture (Van der Veen, 1998; MacAyeal and Sergienko, 2013).

Among the impacts of supraglacial lakes on both grounded and floating ice, none are so powerfully linked to ice sheet change as those leading to the sudden collapse of the Larsen B Ice Shelf (LBIS) in 2002 (*e.g.,* Scambos and others, 2000; 2003; van den Broeke, 2005; Vaughan, 2008). During the decades leading up to the collapse, the number of lakes on the central portion of the ice shelf gradually grew from near zero to ~3000 (Scambos and others, 2000; Glasser and Scambos, 2008). However, just days prior to the disintegration, the majority of the ~3000 lakes drained, suggesting that the sudden, coordinated movement of surface water to the ocean below may have been a contributing proximal trigger to the collapse (Scambos and others, 2003). The loss of the majority of the LBIS resulted in a reduction of buttressing forces that act to reduce ice flow across grounding lines shared with the ice shelf. Following the break-up event, a sustained speed-up of land-to-sea ice flow of glaciers that were previously buttressed by the ice shelf was observed (Scambos and others, 2000; 2004; Sergienko and MacAyeal, 2005; van den Broeke, 2005; Glasser and Scambos, 2008; Glasser and others, 2011; Rott and others, 2011). Thus, as with the acceleration of GrIS flow, the inland ice of Antarctica can also accelerate in response to lake drainage, but by a different mechanism.

However, while ground-based study of supraglacial lakes on the GrIS is increasing in abundance, relatively little ground-based research has been directed toward study of supraglacial lakes on Antarctic ice shelves. Antarctic lakes are harder to study because they are either more remote (relative to logistics centres) or have themselves disappeared as the ice shelves on which they resided no longer exist.

In the present study, we endeavour to strengthen the link between the relatively plentiful research directed to lakes on the GrIS and the relatively unstudied lakes on the present and recently collapsed ice shelves of Antarctica. The first step in establishing this link is to determine parallels and contrasts between spatial patterns, shapes, surface areas, and depths of lakes on the land-terminating Paakitsoq region of the GrIS and on the former LBIS. Our study is conducted through the analysis of Landsat 7 Enhanced Thematic Mapper Plus (ETM+) imagery acquired for both regions.

In addition to improving our overall understanding of supraglacial lakes on ice shelves, this study will help to establish whether or not surface routing and lake filling models which are already in existence for the GrIS (e.g., Banwell and others, 2012a; Leeson and others, 2012) are transferable to Antarctic ice shelves. Finally, our work will establish idealized properties of supraglacial lake geometries; an important first step in the development of numerical model studies of lakes on ice sheets and ice shelves.

2 METHODS

In this section we describe the analytical process that was undertaken for both the LBIS, and for a similar sized (~3000 km^2 area) of grounded ice in the Paakitsoq region of the GrIS, north-east of Jakobshavn Isbrae (see Banwell and others (2012b), their Figure 1). Two Landsat-7 ETM+ images were analyzed as part of this study. For the LBIS, we chose the image dated 21 February 2000 (Scene ID: L71216106_10620000221) as this is the most cloud-free image available within two years of the break-up event. This image also forms the basis of a prior study of lake patterning and morphology on LBIS (Glasser and Scambos, 2008), and thus serves as a fiduciary representation of the state of LBIS two years prior to its collapse. For Paakitsoq, Greenland, we used the cloud-free image dated 7 July 2001 (Scene ID: L71009011_01120010707). We note that the two images are from periods of time during the melt season that do not coincide with either 'time of maximum lake volume' or 'end of season', or any other benchmark, but are rather snap-shots of time that represent the best available information.

2.1. Lake boundaries and area

Image pixels were classified into 'lake covered' or 'bare ice/snow' using Landsat image reflectance data following Box and Ski (2007). Each Landsat band was first converted from digital numbers to radiance and then from radiance to reflectance using the equations of Chander and others (2009). Then, to make this classification, the blue/red ratio of reflectance (involving Landsat bands 1 and 3; 450–515 nm and 630-690 nm, respectively) was evaluated from the Landsat image. As this ratio increases toward the lake centres, where water is deepest, and decreases towards the edges, where water is most shallow, it was necessary to carefully identify the value of this ratio corresponding to bare ice at lake edges. Based on experimental results, and on known areas of lakes on the GrIS, Box and Ski (2007) suggest that the threshold value of blue/red ratio of reflectance should be in the range of 1.05-1.25 at the edges of lakes. Further to the study by Box and Ski (2007), we found that the algorithm needed to be adapted to avoid problems associated with floating lake ice on lake surfaces. Unless these areas were masked, negative lake depths were found due to the high reflectance of the ice compared to the open water.

Once the pixels representing flooded areas had been established, the 'bwboundaries' function in MATLAB was used to identify lake boundaries. Subsequently, the 'regionprops' function in MATLAB was used to identify the number of pixels (i.e., surface areas of lakes) within the closed edges as a means of determining lake area.

2.2. Lake depth

Supraglacial lake depths were estimated using a method developed by Sneed and Hamilton (2007), originally applied to Advanced Spaceborne Thermal Emission and Reflection Radiometer (ASTER) (VNIR1, 520–600 nm) imagery, but also applicable to Landsat 7 ETM+ imagery (Band 2; 525–605 nm) (Sneed and Hamilton, 2011). The approach for extracting water depth and lake-bottom albedo is based on the Beer-Lambert law (Ingle and Crouch, 1988), which describes the attenuation of radiation through a water column:

$$I(z,\lambda) = I(0,\lambda)e^{-(K_\lambda)(z)}, \qquad \text{(Eqn. 1)}$$

where $I(z,\lambda)$ is the water-leaving spectral intensity at some depth, $I(0,\lambda)$ is the spectral intensity at zero depth, K_λ is the spectral attenuation, and z is depth. Written in terms of reflectance, and inverted to logarithmic form (Philpot, 1989), z is determined by

$$\mathrm{z} = [\ln(A_\mathrm{d} - R_\infty) - \ln(R_\mathrm{w} - R_\infty)]/(1 - g) \qquad \text{(Eqn. 2)}$$

where A_d is the bottom or substrate albedo (reflectance), R_∞ is the reflectance for optically deep water, R_w is the reflectance of some pixel of interest, and g is given by

$$g \approx K_d + aD_u \qquad \text{(Eqn. 3)}$$

where K_d is the diffuse attenuation coefficient for downwelling light, a is the beam absorption coefficient, and D_u is an upwelling light distribution function or the reciprocal of the upwelling average cosine (Mobley, 1994).

To determine A_d, the bottom or substrate albedo, we took the mean reflectance value of the ring of pixels around the lake that are barely covered with water (i.e. those adjacent to the water-covered pixels, as detected by the blue/red ratio of reflectance). Although Sneed and Hamilton (2007) used the same A_d for their entire region of interest, as our region is larger, we chose to calculate a unique A_d for each lake. For the LBIS, values for A_d ranged from 0.30 to 0.79 (with a mean value of 0.68), and for Paakitsoq, values for A_d ranged from 0.17 to 0.76 (with a mean value of 0.66).

To determine R_∞, the reflectance from optically deep water where the influence of bottom reflectance is nil, we used the value of reflectance from water that is deeper than ~40 m in the image. It was necessary to take care when selecting pixels that were far from shorelines to insure that R estimates were not biased by water that was too shallow, turbid water, or pixels containing floating ice.

This approach assumes that the substrate (bottom) of the lake is homogeneous, the impact of suspended or dissolved organic or inorganic matter in the water column is negligible on absorption, there is no inelastic scattering (e.g., Raman scattering or fluorescence), and that the lake surface is not significantly rough due to wind (Sneed and Hamilton, 2007). Once the depth of each 'flooded' pixel had been calculated, the 'regionprops' function in MATLAB was again used to determine the 'MaxIntensity' (i.e., the maximum lake depth), and the 'MeanIntensity' (i.e., the mean lake depth) for each of the identified lakes.

2.3. Lake shape, orientation and eccentricity

Once lake edges, and thus areas, had been delineated (following Box and Ski, 2007), and depths had been established (following Sneed and Hamilton, 2007), the MATLAB 'regionprops' function was used to obtain other lake properties. As illustrated in Figure 1, this function works by best-fitting ellipses to the identified lakes. Lake properties which this function is able to diagnose include: (i) eccentricity (i.e., the ratio from 0-1 of the distance between the foci of the ellipse and its long axis length; where 0 indicates that the ellipse is a circle, and 1 indicates a line segment); (ii) orientation (from 0° to 90° from the average ice flow direction on the ice shelf/sheet in either a clockwise or anti-clockwise direction); and iii) solidity (from 0-1; denoting the proportion of the pixels in the convex hull of the lake that are also bound within the lake itself, lakes with sinuous boundaries tend to have low solidity, circular lakes have a solidity of 1).

2.4. Algorithm validation

Using the same 21 February 2000 image, Glasser and Scambos (2008) produced a detailed structural glaciological analysis of overall changes in surface structures on the LBIS prior to its collapse in late February 2002. Although this study, which used manual digitization, identified general patterns of lake positions, areas and shapes of supraglacial lakes, it did not perform a quantitative analysis of these properties, and importantly did not analyze lake depth. Thus, in our study, we also statistically analyze the shape files of lakes used in the Glasser and Scambos (2008) study in order to compare, and thus validate, the results of our study using an automated algorithm.

3. RESULTS

3.1. Larsen B lake patterns and characteristics

The most appropriate value for the blue/red band threshold for the LBIS to appropriately discriminate bare ice/snow from water is found to be 1.2, which results in the identification of 3227 lakes, as shown in Figure 2. This threshold value is chosen because it produces a pattern of lakes on the ice-shelf surface that is most similar to the pattern of lakes identified visually on the Landsat image, and documented by Glasser and Scambos (2008) (also see Section 3.2 below). If a slightly lower threshold value of 1.1 is chosen, only 272 separate flooded areas are identified as the majority of the entire surface of the LBIS is erroneously classified as lake-covered. If a slightly higher threshold value of 1.3 is chosen, only 1419 lakes are identified, and the small lakes, in particular, are no longer identified.

As also recognized by Glasser and Scambos (2008), we identify a variety of different 'domains' on the ice-shelf surface, each displaying different lake characteristics. We have highlighted lakes within three areas of these domains in Figure 2. In area 'a' of Figure 2, we see fairly linearly shaped lakes, with their long axis diverging from the mean ice flow direction from west to east. This is indicative of ice flow divergence where fast-flowing glaciers enter the ice shelf from the west. Although lake depths generally vary from ~1 to ~4 m here, the deepest identified lake on the ice shelf also falls within this region; calculated to be 6.8 m at it's deepest point. In area 'b' of Figure 2, longitudinal features, which are aligned roughly parallel with ice flow, dominate. These features are up to 30 km in length and 2 to 3 m in depth. Thus, compared to area 'a', ice flow in this region is likely to be convergent rather than divergent along the flow direction. In area 'c' of Figure 2, we see lakes that are fairly circular (i.e., their eccentricity is close to 1) and have a larger mean area compared to the majority of lakes on the ice shelf. We suggest that these characteristics are due to slower ice flow in this region (for additional information on structural features of the LBIS related to flow, as well as the area of the LBIS that disintegrated, refer to Glasser and Scambos, 2008). Through an increased lifespan, lakes would be able to undergo more enlargement by bottom ablation than other lakes on the ice shelf. The majority of the lakes in this area are also covered with floating ice (seen as white areas in Figure 2c). Although the outer rings of open, lake-ice-free water of the lakes are calculated to be from ~0.5 to ~1.5 m in depth, we cannot calculate the depth of the central, likely deepest, regions because of the ice cover.

Over the entire ice shelf, we calculate the mean lake area to be 0.10 km^2 (standard deviation = 0.29 km^2), and the total surface area covered by lakes to be 315 km^2. This is 5.3% of the total area of ice shelf analyzed, with a mean lake density of 0.55 km^{-2}. Of the 3,200 km^2 of ice shelf area which disintegrated in a 35-day period beginning on 31 January 2002 (Scambos and others, 2004), we calculate that lakes covered ~10% of this. As we will discuss below, this larger percentage of lake cover constitutes one of the most important differences between lakes on the LBIS and lakes on the GrIS.

The mean lake depth on the LBIS is calculated to be 0.82 m (standard deviation = 0.56 m), and the mean maximum lake depth is 1.6 m (standard deviation = 0.99 m) (Figure 3). The mean eccentricity is 0.84 (standard deviation = 0.13 m), the mean solidity is 0.80 (standard deviation = 0.14), and the average mean orientation of the long axis of ellipses (best-fitted to the lakes) is 46° away from the flow direction (standard deviation = 28°). The latter assumes that the average flow direction is from west to east (Vieli and others, 2006, their Figure 5).

Using the mean lake depth (0.82 m), the total number of lakes on the LBIS (3227), the average lake area (0.1 km^2), and the assumption that the ice shelf has a uniform thickness of 200 m (Sandhäger and others, 2005), we calculate that there are 5.2 x 10^8 MJ of potential energy stored on the surface as free water (equivalent to 8.7 x 10^4 MJ per km^2). This calculation is useful as it gives an indication of the amount of energy available for the drainage of lakes by hydrofracture; the process that was likely the main driver behind the disintegration of the ice shelf (Scambos and others, 2003; 2009).

3.2. Comparison to results of the Glasser and Scambos (2008) study

Glasser and Scambos (2008) identified 2696 supraglacial lakes (their 'meltwater ponds'); 16% fewer than the number of lakes identified in our study. Glasser and Scambos (2008) also calculated that individual lakes had a slightly higher mean area of 0.13 km^2, and in total, they calculated that lakes on the LBIS covered a slightly higher surface area of 365 km^2. However, although we calculate that lakes are on average ~30% smaller than the lakes identified by Glasser and Scambos (2008), as we identify ~16% more lakes on the LBIS than Glasser and Scambos (2008), we calculate that the total surface area of lake coverage is only ~12% less than that calculated by Glasser and Scambos (2008).

3.3. Comparison with a land-terminating region of the GrIS

Compared to the threshold value for the blue/red ratio for the LBIS, a slightly higher threshold value of 1.4 is required for the Paakitsoq region of the GrIS. Using this threshold value, we identified 239 lakes, as shown in Figure 4 (note the different scale to Figure 1). Threshold values <1.4 for Paakitsoq result in large, dispersed areas of the ablation zone to be erroneously classified as lakes. Threshold values >1.4 for Paakitsoq meant that the wispy, linear water features, observed to link lakes in the areas of higher elevation within the region studied (see Figure 4, area ‘b’), were no longer identified as flooded areas.

Figure 3 compares the values of key lake properties between the LBIS and the Paakitsoq region. Compared to lakes on the LBIS, lakes in the Paakitsoq region have a larger mean area of 0.15 km^2 (standard deviation = 0.24 km^2). However, we calculate that lakes only cover ~1% of the ice surface compared to 5.3% for the LBIS. The mean lake density in the Paakitsoq region is thus only 0.07 km^{-2}. This constitutes one of the major differences between lakes on grounded ice and floating ice we have identified in the comparison.

Lakes in the Paakitsoq region are also generally deeper than lakes on the LBIS with a mean depth of 1.3 m (standard deviation = 0.97 m) and a mean maximum depth of 2.5 m (standard deviation = 1.9 m) (Figures 3 and 4). The deepest identified lake in the region, calculated to have a maximum depth of 9.0 m, is shown in area ‘a’ within Figure 4. Overall, lake depths across the Paakitsoq region show more variation than the lakes on the LBIS (Figure 3). With regard to the lake orientations, LBIS lakes are on average orientated 51° away from the dominant ice flow direction, whereas the average orientation of Paakitsoq lakes from the dominant flow direction (east to west) is 37° (standard deviation = 24°). The calculated solidity for the Paakitsoq lakes is 0.83 (standard deviation = 0.15), which is 4% higher than the value for the LBIS lakes (i.e., Paakitsoq lakes are more convex than LBIS lakes).

4. DISCUSSION

When average values for lake properties identified in our study are compared to those of lakes identified by Glasser and Scambos (2008), it is encouraging that the total number of lakes and the average area of those lakes are of the same order of magnitude for both studies. There are, however, some minor discrepancies. For example, we identify 16% more lakes than Glasser and Scambos (2008), and those lakes are on average 30% smaller. Thus, it is likely that Glasser and Scambos' (2008) analysis may have grouped together into one large lake what our automated algorithm identified as a collection of nearby smaller lakes.

The automated algorithm used in our study extends the Glasser and Scambos (2008) study by also calculating lake depths. Glasser and Scambos (2008) state that although supraglacial lakes are generally aligned along the local topographic slope (which is roughly aligned perpendicular to the general ice flow direction), some surface water features are longitudinal in form and are aligned parallel to the downslope direction. Although they suggested that these features could be interpreted as meltwater streams, as have been observed on the Amery Ice shelf (Phillips, 1998), such a deduction does not agree with all other observations. For example, as we calculate these features to be ~2 m or more deep (Figure 2, area 'b', displayed in a light green colour), we suggest that they are unlikely to all be meltwater streams as many do not reach the eastern edge of the ice shelf and thus there is not an obvious outflow point for a large quantity of water to leave the ice shelf (unless outflow is accommodated by a moulin). Additionally, as the ice shelf surface slope is minimal (i.e., the ice thickness change from grounding line to ice front is roughly 50 m (Sandhäger and others, 2005, their Figure 2), implying a 5 m change in ~50 km, or a slope of 10^{-4}), it seems unlikely that there could be a substantial volume of flowing water across the ice shelf surface. Thus, although some meltwater has been observed to leave the LBIS as waterfalls (T. Scambos, pers. comm.), this runoff into the ocean is likely to be only a small fraction of the summer surface melt volume.

The standard deviations of mean lake depth, maximum lake depth, and lake area are generally higher in the Paakitsoq region, indicating that Paakitsoq lakes have more variable depths and areas than LBIS lakes. The reason for this is likely to be primarily related to the substantial elevation gradient in the Paakitsoq region; from about 400 m at the ice margin to 1500 m inland, compared to an almost negligible elevation gradient on the floating LBIS. Consequentially, on the GrIS, increased melt as summer progresses not only causes existing lakes to grow, but it also results in lake formation at higher elevations as the ablation zone expands (Liang and others, 2012; Fitzpatrick and others, 2013). Conversely, the standard deviations of eccentricity, orientation, and solidity are found to be comparable between the two regions. This is because these lake properties are affected by elevation to a much lesser extent than lake depth and area.

The mean depth of Paakitsoq lakes is calculated to be 0.48 m more than for lakes on the LBIS, and the mean maximum depth of Paakitsoq lakes is calculated to be 0.90 m more than LBIS lakes (Figure 3). Additionally, Paakitsoq lakes are on average 0.05 km^2 larger than LBIS lakes. A less striking difference between lakes in the two regions concerns their average orientation. We calculate that Paakitsoq lakes are orientated at a lower angle (37°) to the average ice flow direction than LBIS lakes are (46°). These differences are thought to be due to a variety of different reasons, discussed below.

We suggest that the differences in average lake depth and area are partially due to the higher surface melt rates on the GrIS. Owing to its sheer size and elevation, the

Antarctic Ice Sheet creates its own climate with an important influence on the surrounding ocean (Rignot and Thomas, 2002; Bromwich and others, 2012). Furthermore, once a lake exists, it enlarges not only by receiving meltwater from the surrounding ice surface, but also due to a positive albedo feedback process whereby bottom-lake ablation is enhanced by up to 170% compared to bare ice, as modelled by Luthje and others (2006), and up to 135%, as observed by Tedesco and others (2012).

The other reason for the differences in average lake depth, area, and orientation between the two locations relates to the two fundamentally different ways in which supraglacial lakes on land-terminating regions of the GrIS and on Antarctic ice shelves initially form and subsequently interact with one another. At Paakitsoq, supraglacial lakes form in surface depressions that are controlled by the underlying bedrock topography (Box and Ski, 2007; Lampkin and Vanderberg, 2011) and by spatial variations in the degree of basal ice lubrication and sliding velocity (Gudmundsson, 2003). This causes the majority of lakes on the GrIS to remain in fixed locations interannually (Thomsen and others, 1988; Echelmeyer and others, 1991; Selmes and others, 2011), and thus the average orientation and volume of lakes in a specific region of the GrIS will depend on the average patterns of bed topography and basal friction in that region. Additionally, if lakes on the GrIS overflow, lakes in downstream catchments may receive extra water, and thus surface catchment areas of lakes on the GrIS may enlarge through the melt season (Banwell and others, 2012a).

Conversely, undulations and depressions on ice shelves, which may fill to form lakes, are produced and influenced by an entirely different combination of processes. To date, only a few previous studies have focused on improving our understanding of lake formation processes on ice shelves. One such study is that by LaBarbera and MacAyeal (2011) who suggest that supraglacial lakes on ice shelves form in the depressions of a viscous-buckling wave associated with compressive ice shelf stresses. This idea is thought to be associated with a previously described ice shelf phenomenon known as 'pressure rolls' (Hattersley-Smith, 1957; Collins and McCrae, 1985). As various studies have also concluded, when supraglacial lakes accumulate water, they begin to flex the ice shelf downward, causing further deepening and attraction of surrounding meltwater runoff patterns (Hattersley-Smith, 1957; MacAyeal and Sergienko, 2013). However, due to the minimal surface slope of ice shelves compared to the steep surface slope of the GrIS, only relatively small catchment areas are likely to develop on ice shelves.

Further to these ideas, we speculate that surface undulations on ice shelves may form as ice crosses the sudden break in slope at the grounding line, as here it is likely to experience some degree of flexure, buckling, or fracturing. For example, ice-covered lakes and dolines were observed near the grounding line of the Lambert/Amery Ice Shelf by Hambrey and Dowdeswell (1994). It is also here (i.e. near the Antarctic Peninsula mountains) where surface melting is likely to be highest, owing to a fohn effect and/or runoff from darker, ice-free areas. As the ice subsequently converges away from the grounding line and out onto the ice shelf and towards the ice front, these undulations, which were likely parallel to the grounding line (if the ice flow direction was perpendicular to the grounding line), may undergo strain and thus rotation in response to the convergence of ice flow and the resultant stress field. We suggest that it is the combination of these processes that assist in producing lakes on the LBIS which are relatively shallow and uniform in depth, and have an average orientation of 46° to the general ice flow direction.

5. CONCLUSIONS

Compared to lakes at Paakitsoq, a land-terminating region of the GrIS, lakes on the floating LBIS show less variance in their mean depths and areas. It is therefore conceivable that the majority of lakes on the LBIS all reached a critical volume to drain by hydrofracture at a similar time, enabling the rapid break-up of the ice shelf in March 2002. Compared to lakes at Paakitsoq, lakes on the LBIS have a greater spatial density, and also cover a greater proportion of the total surface area of the ice on which the lakes are localized (~5.3 % vs. ~1.0 %). This greater density is likely due to the almost negligible large-scale elevation change across the surface of the ice shelf (~25 m) compared to a change on the order of ~1100 m at Paakitsoq. As a consequence of the low variability of the surface elevation of the LBIS, it seems feasible that supraglacial lakes are hydrologically isolated (i.e., where water does not overflow from basins of different elevation) and simply grow in place by enhanced surface ablation associated with the reduced albedo of standing water.

Finally, if we consider the transferability of existing surface routing and lake filling models (e.g., Banwell and others, 2012a; Leeson and others, 2012), to Antarctic ice shelves, we conclude that ice shelves are likely to be too flat to enable the widespread movement of meltwater across the surface and the filling of surface depressions to be coherently modelled. This likely means that lakes on ice shelves can be modelled more simplistically as features that derive their water from local drainage basins that are relatively static in size and shape. Additionally, existing surface routing and lake filling models assume static ice topography. Although this is a suitable assumption for the GrIS where lake positions are relatively constant interannually, this is not a suitable assumption for Antarctic ice shelves where lakes move concurrently with ice flow and where lake water constitutes a surface load that introduces vertical flexure.

ACKNOWLEDGMENTS

We acknowledge the support of the U.S. National Science Foundation under grant ANT-0944248. We also thank the scientific editor, Weli Wang, and two anonymous referees for careful reviews that helped to improve an earlier draft of the paper.

REFERENCES

Banwell, A. F., N. S. Arnold, I. C. Willis, M. Tedesco and A. P. Ahlstrøm (2012a), Modeling supraglacial water routing and lake filling on the Greenland Ice Sheet, *J. Geophys. Res., Earth Surf.,* 117, F04012, doi: 10.1029/2012JF002393.

Banwell, A. F., I. Willis, N. Arnold, A. Messerli, C. Rye and A. Ahlstrom (2012b), Calibration and validation of a high resolution surface mass balance model for Paakitsoq, west Greenland, *J. Glaciol.* 58(212), 1047–1062. doi:10.3189/2012JoG12J034.

Banwell, A. F., I. Willis and N. Arnold (2013), Modeling subglacial water routing at Paakitsoq, W Greenland. *J. Geophys. Res. Earth Surf., 118,* doi:10.1002/jgrf.20093

Bartholomew, I., P. Nienow, A. Sole, D. Mair, T. Cowton, M. King and S. Palmer (2011), Seasonal variations in Greenland Ice Sheet motion: inland extent and behaviour at higher elevations. *Earth Planet. Sci. Lett.*, 307, 271-278, doi:10.1016/j.epsl.2011.04.014.

Box, J. E., and K. Ski (2007), Remote sounding of Greenland supraglacial melt lakes: implications for subglacial hydraulics, *J. Glaciol.*, 53(181), 257–265, doi:10.3189/172756507782202883.

Bromwich, D. H., J. P. Nicolas, A. J. Monaghan, M. A. Lazzara, L. M. Keller, G. A. Weidner and A. B. Wilson (2012), Central West Antarctica among the most rapidly warming regions on Earth, *Nat. Geos.,* 6, 139-145, doi:10.1038/ngeo1671.

Chander G, B. L. Markham and D. L. Helder (2009), Summary of current radiometric calibration coefficients for Landsat MSS, TM, ETM+, and EO-1 ALI sensors. *Remote Sens. Environ.*, 113(5), 893–903. doi: 10.1016/j.rse.2009.01.007.

Collins, I. F., and I. R. McCrae (1985), Creep buckling of ice shelves and the formation of pressure rollers, *J. Glaciol.* 31(109), 242–252.

Darnell, K., J. M. Admundson, L. M. Cathles and D. MacAyeal (2013), The morphology of supraglacial lake ogives , *J. Glaciol.,* 59(215), 533-544, doi:10.3189/2013JoG12J098

Das, S. B., I. Joughin, M. Behn, I. Howat, M. King, D. Lizarralde and M. P. Bhatia (2008), Fracture Propagation to the Base of the Greenland Ice Sheet during Supraglacial Lake Drainage, *Science,* 320, 778–781. doi:10.1126/science.1153360.

Doyle, S. H., A. L. Hubbard, C. F. Dow, G. A. Jones, A. Fitzpatrick, A. Gusmeroli, B. Kulessa, K. Lindback, R. Pettersson and J. E. Box (2013), Ice tectonic deformation during the rapid in situ drainage of a supraglacial lake on the Greenland Ice Sheet, *Cryosphere,* 7, 129–140, 25, doi:10.5194/tc-7-129-2013.

Echelmeyer, K., T. S. Clarke and W. D. Harrison (1991), Surficial glaciology of Jakobshavns Isbræ, west Greenland: I. Surface morphology, *J. Glaciol.,* 37(127), 368–382.

Fitzpatrick, A. A. W., A. L. Hubbard, J. E. Box, D. J. Quincey, D. van As, A. P. V. Mikkelsen, S. H. Doyle, C. F. Dow, B. Hasholt and G. A. Jones (2013), A decade of supraglacial lake volume estimates across a land-terminating margin of the Greenland Ice Sheet, *Cryosphere Discuss.,* 7, 1383-1414, doi:10.5194/tcd-7-1383-2013.

Glasser, N. F., and T. A. Scambos (2008), A structural glaciological analysis of the 2002 Larsen B Ice Shelf collapse, *J. Glaciol.*, 54(184), 3-16.

Glasser, N. F., B. Kulessa, A. Luckman, D. Jansen, E. C. King, P. R. Sammonds, T. A. Scambos and K. C. Jezek (2009), Surface structure and stability of the Larsen C ice shelf, Antarctic Peninsula, *J. Glaciol.,* 55(191), 400-410.

Glasser, N. F., T. A. Scambos, J. Bohlander, M. Truffer, E. Pettit, and B. J. Davies (2011), From ice-shelf tributary to tidewater glacier: continued rapid recession, acceleration and thinning of Rohss Glacier following the 1995 collapse of the Prince Gustav Ice Shelf, Antarctic Peninsula, *J. Glaciol.,* 57, 397–406, doi:10.3189/002214311796905578.

Glasser, N. F., and G. H. Gudmundsson (2012), Longitudinal surface structures (flowstripes) on Antarctic glaciers, *Cryosphere*, 6, 383-391, doi: 10.5194/tc-6-383-2012.

Gudmundsson, G.H., (2003), Transmission of basal variability to a glacier surface. *J. Geophys. Res.,* 108(B5), 2253 doi:10.1029/2002JB0022107.

Hambrey, M. J., and J. A. Dowdeswell (1994), Flow regime of the Lambert Glacier-Amery Ice Shelf system, Antarctica: structural evidence from Landsat imagery, *Ann. Glaciol.,* 20, 401–406.

Hattersley-Smith, G. (1957), The rolls on the Ellesmere Ice Shelf, *Arctic*, 10(1), 32–44.

Hoffman, M. J., G. A. Catania, T. A. Neumann, L. C. Andrews and J. A. Rumrill (2011), Link between acceleration, melting, and supraglacial lake drainage of the western Greenland Ice Sheet, *J. Geophys. Res.,* 116, F04035.

Ingle, J. D. J., and S. R. Crouch (1988), Spectrochemical measurements, in Spectrochemical Analysis, Prentice Hall, New Jersey, USA.

Johansson, A. M., P. Jansson and I.A. Brow (2013), Spatial and temporal variations in lakes on the Greenland Ice Sheet, *J. Hydrol.*, 476, 314-32.

Joughin, I., S. B., Das, G. E. Flowers, M. D. Behn, R. B. Alley, M. A. King, B. E. Smith, J. Bamber, M. R. van den Broeke and J. H. van Angelen (2013), Influence of supraglacial lakes and ice-sheet geometry on seasonal ice-flow variability, *Cryosphere Discuss.*, 7, 1101-1118, doi:10.5194/tcd-7-1101-2013.

LaBarbera, C. H., and D. R. MacAyeal (2011), Traveling supraglacial lakes on George VI Ice Shelf, Antarctica, *Geophys. Res. Lett.,* 38, L24501, doi:10.1029/2011GL049970.

Lampkin, D. J., and J. Vanderberg (2011), A preliminary investigation of the influence of basal and surface topography on supraglacial lake distribution near Jakobshavn Isbræ, *Hydrol. Processes*, doi:10.1002/hyp.8170.

Leeson, A. A., A. Shepherd, S. Palmer, A. Sundal and X. Fettweis (2012), Simulating the growth of supraglacial lakes at the western margin of the Greenland ice sheet, *Cryosphere,* 6, 1077-1086, doi:10.5194/tc-6-1077-2012.

Liang, Y., W. Colgan, L. Qin, K. Steffen, W. Abdalati, J. Stroeve, D. Gallagher and N. Bayou (2012), A decadal investigation of supraglacial lakes in West Greenland using a fully automatic detection and tracking algorithm. *Remote Sens. Environ.,* 123, 127-138.

Luthje, M., L. T. Pedersen, N. Reeh and W. Greuell (2006), Modelling the evolution of supraglacial lakes on the West Greenland ice-sheet margin, *J. Glaciol.*, 52, 608–618.

MacAyeal, D.R., T.A. Scambos, C.L. Hulbe and M.A. Fahnestock (2003), Catastrophic ice-shelf break-up by an ice-shelf-fragment- capsize mechanism. *J. Glaciol.,* 49(164), 22–36.

MacAyeal, D. R. and O. V. Sergienko (2013), The flexural dynamics of melting ice shelves, *Ann. Glaciol.,* 54(63), 1-10, doi: 10.3189AoG63A256.

McGrath, D., K. Steffen, H. Rajaram, T. Scambos, W. Abdalati and E. Rignot (2012), Basal crevasses on the Larsen C Ice Shelf, Antarctica: Implicaitons for meltwater ponding and hydrofracture, *Geophys. Res. Lett.,* 39(16), L16504, doi:10.1029/2012GL052413.

Mobley, C. D. (1994), Light and water: radiative transfer in natural waters. Academic Press, San Diego, 592.

Phillips, H. A. (1998), Surface meltstreams on the Amery Ice Shelf, East Antarctica, *Ann. Glaciol.,* 27(1) 177-181.

Rignot, E., and R. H. Thomas (2002), Mass balance of polar ice sheets, *Science*, 297,1502–1506.

Rott, H., F. Müller, T. Nagler and D. Floricioiu (2011), The Imbalance of glaciers after disintegration of Larsen B ice shelf, Antarctic Peninsula. *Cryosphere*, 5, 125-134, doi:10.5194/tc-5-125-2011.

Sandhager, H., W. Rack and D. Jansen (2005), Model investigations of Larsen B Ice Shelf dynamics prior to the breakup. FRISP Rep. 16, 5–12

Scambos, T.A., C. Hulbe, M. Fahnestock and J. Bohlander (2000), The link between climate warming and break-up of ice shelves in the Antarctic Peninsula, *J. Glaciol.,* 46(154), 516–530.

Scambos, T. A., C. Hulbe and M. A. Fahnestock (2003), Climate-induced ice shelf disintegration in the Antarctic Peninsula. *Antarctic Research Series* 79: 79-92.

Scambos, T. A., J. Bohlander, C. Shuman and P. Skvarca (2004), Glacier acceleration and thinning after ice shelf collapse in the Larsen B embayment, Antarctica. *Geophys. Res. Letts.* 31, L18402, doi:10.1029/2004GL020670.

Scambos, T., H. A. Fricker, C.-C. Liu, J. Bohlander, J. Fastook, A. Sargent, R. Massom and A.-M. Wu (2009), Ice shelf disintegration by plate bending and hydro-fracture: Satellite observations and model results of the 2008 Wilkins ice shelf break-ups, *Earth and Plan. Sci. Lett.*, 280, 51-60.

Selmes, N., T. Murray and T. D. James (2011), Fast draining lakes on the Greenland Ice Sheet, *Geophys. Res. Lett.,* 38, L15501, doi:10.1029/2011GL047872.

Selmes, N., T. Murray and T. D. James (2013), Characterizing supraglacial lake drainage and freezing on the Greenland Ice Sheet, *Cryosphere Discuss.,* 7, 475-505, doi:10.5194/tcd-7-475-2013.

Sergienko, O. V., and D.R. MacAyeal (2005), Surface melting on Larsen ice shelf, Antarctica, *Ann. of Glaciol.*, 40(10), 215-218.

Sergienko, O. V. (2013), Glaciological twins: basally controlled subglacial and supraglacial lakes, *J. Glaciol*, 59(213), 3-8, doi:10.3189/2013JoG12J040.

Shepherd, A., D. Wingham, and E. Rignot (2004), Warm ocean is eroding West Antarctic Ice Sheet, *Geophys. Res. Lett.,* 31, L23402, doi:10.1029/ 2004GL021106.

Sneed, W. A., and G. S. Hamilton (2007), Evolution of melt pond volume on the surface of the Greenland Ice Sheet, *Geophys. Res. Lett.*, 34(3), L03501, doi: 10.1029/2006GL028697.

Sneed, W.A. and G.S. Hamilton, (2011), Validation of a method for determining the depth of glacial melt ponds using satellite imagery. *Ann. Glaciol.,* 59, 15-22.

Tedesco, M., M. Luthje, K. Steffen, X. Fettweis, I. Willis, N. Steiner, N. Bayou, and A. Banwell (2012), Measurement and modeling of ablation of the bottom of supraglacial lakes in Western Greenland, *Geophys. Res. Lett.,* 39, L02502, doi:10.1029/2011GL049882.

Tedesco, M., I. C. Willis, M. J. Hoffman, A. F. Banwell, P. Alexander, and N. S. Arnold (2013), Ice dynamic response to two modes of surface lake drainage on the Greenland ice sheet, *Environ. Res. Lett.,* 8, 034007, doi:10.1088/1748-9326/8/3/034007.

Thomsen, H.H., L. Thorning and R. J. Braithwaite (1988), Glacier-hydrological conditions on the Inland Ice north-east of Jakobshavn/Ilulissat, West Greenland. Rapport Grønlands Geologiske Undersøgelse, 138.

Van den Broeke, M. (2005), Strong surface melting preceded collapse of Antarctic Peninsula ice shelf, *Geophys. Res. Lett.,* 32, 364, L12815, doi:10.1029/2005GL023247.

Van der Veen, C. J. (1998), Fracture mechanics approach to penetration of surface crevasses on glaciers. *Cold Reg. Sci. Technol.,* 27(1), 31–47

Van der Veen, C.J. (2007), Fracture propagation as means of rapidly transferring surface meltwater to the base of glaciers. *Geophys. Res. Lett.,* 34, 1, doi:L01501 10.1029/2006GL028385.

Vaughan, D. G., and C. S. M. Doake (1996), Recent atmospheric warming and retreat of ice shelves on the Antarctic Peninsula, *Nature,* 379, 328-331.

Vaughan, D. G. (2008), West Antarctic Ice Sheet collapse–the fall and rise of a paradigm. *Climatic Change*, *91*(1-2), 65-79.

Vieli, A., A. J. Payne, Z. Du and A. Shepherd (2006), Numerical modelling and data assimilation of the Larsen B ice shelf, Antarctic Peninsula. *Proc. R. Soc. London,* Ser. A 364, 1815–1839.

Weertman, J., (1973), Can a water-filled crevasse reach the bottom surface of a glacier? *IAHS-AISH Publ.,* 95, 139–45.

FIGURES

Figure 1: Schematic of optimal fit of an ellipse to the outline of a previously identified lake. The ellipse and original lake are equal in area. The angle between the long axis of the ellipse and the flow direction (either clockwise or anti-clockwise) determines the ellipse orientation.

Figure 2: Depth (in metres) of lakes on the Larsen B Ice Shelf using reflectance of the 21 February 2000 Landsat image. Although some lake depths are greater than 4 m, for visualization purposes, 4 m is plotted as the maximum depth here. Three areas, ‘a’, ‘b’ and ‘c’, are highlighted to show varying lake characteristics and patterns across the ice shelf surface. Marginal areas, which can be grounded ice, bare land surface or ocean surface, are shaded grey.

Figure 3: Plots showing: i) maximum depth; ii) mean depth; iii) mean area; iv) eccentricity; v) solidity; and vi) orientation from the mean flow direction, of lakes on both the LBIS (N=3227) and at Paakitsoq, W Greenland (N=239) in order to clearly capture the scale and differences of the two lake systems. On each box, the red mark is the median and the edges of the box are the 25th and 75th percentiles (q_1 and q_3, respectively). The length of the whiskers (dotted lines) are equal to $q_3 + 1.5(q_3 - q_1)$.

Figure 4: Depth (in metres) of lakes in the Paakitsoq region, W Greenland (see Banwell and others, 2012b for location figure) using reflectance of the 7 July 2001 Landsat image. Two areas, 'a' and 'b', are highlighted in order to show varying lake characteristics and patterns across the ice sheet surface. Marginal areas of bare land surface are shaded grey.

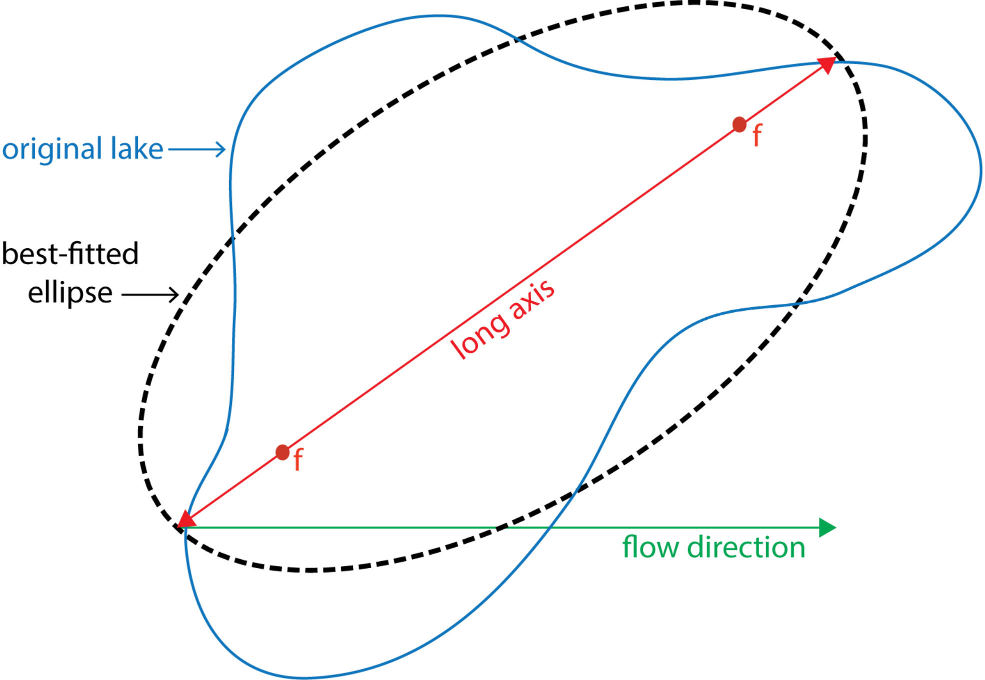
original lake
best-fitted
ellipse
f
f
long axis
flow direction

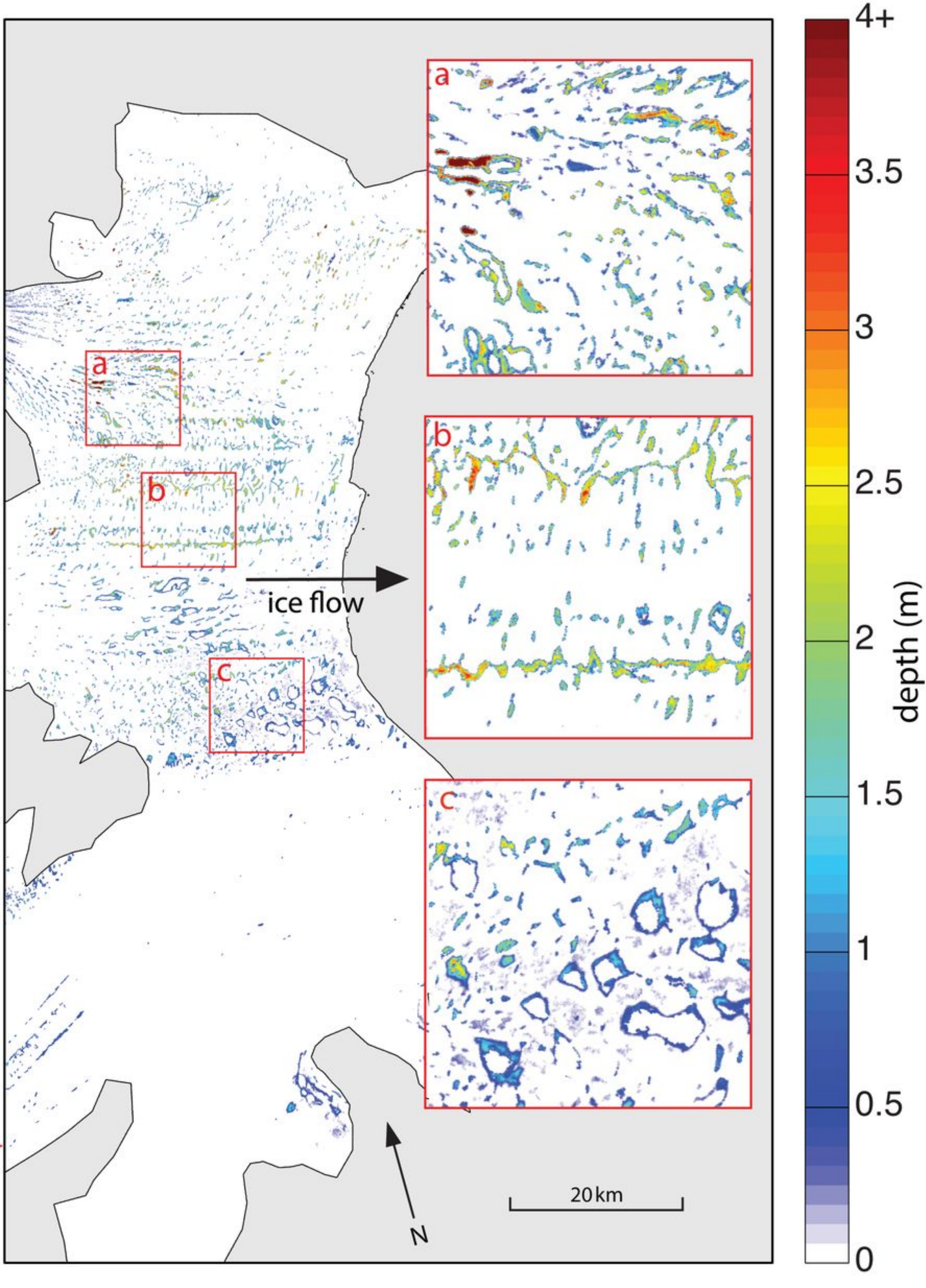

a
b
c
ice flow
20 km
N
4+
3.5
3
2.5
2
1.5
1
0.5
0
depth (m)

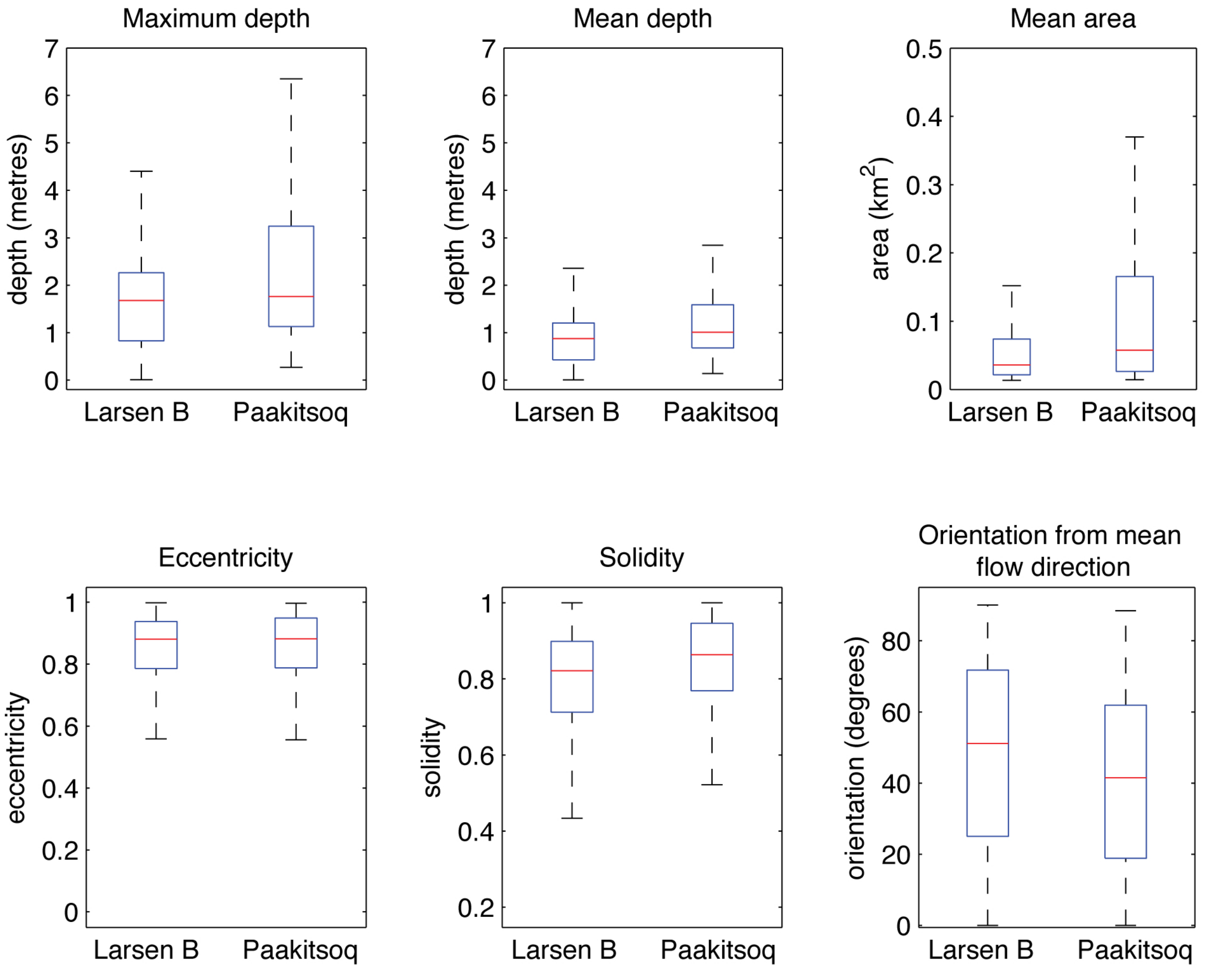
Maximum depth
depth (metres)
Mean depth
depth (metres)
Mean area
area (km2)
Eccentricity
eccentricity
Solidity
solidity
Orientation from mean flow direction
orientation (degrees)
Larsen B
Paakitsoq

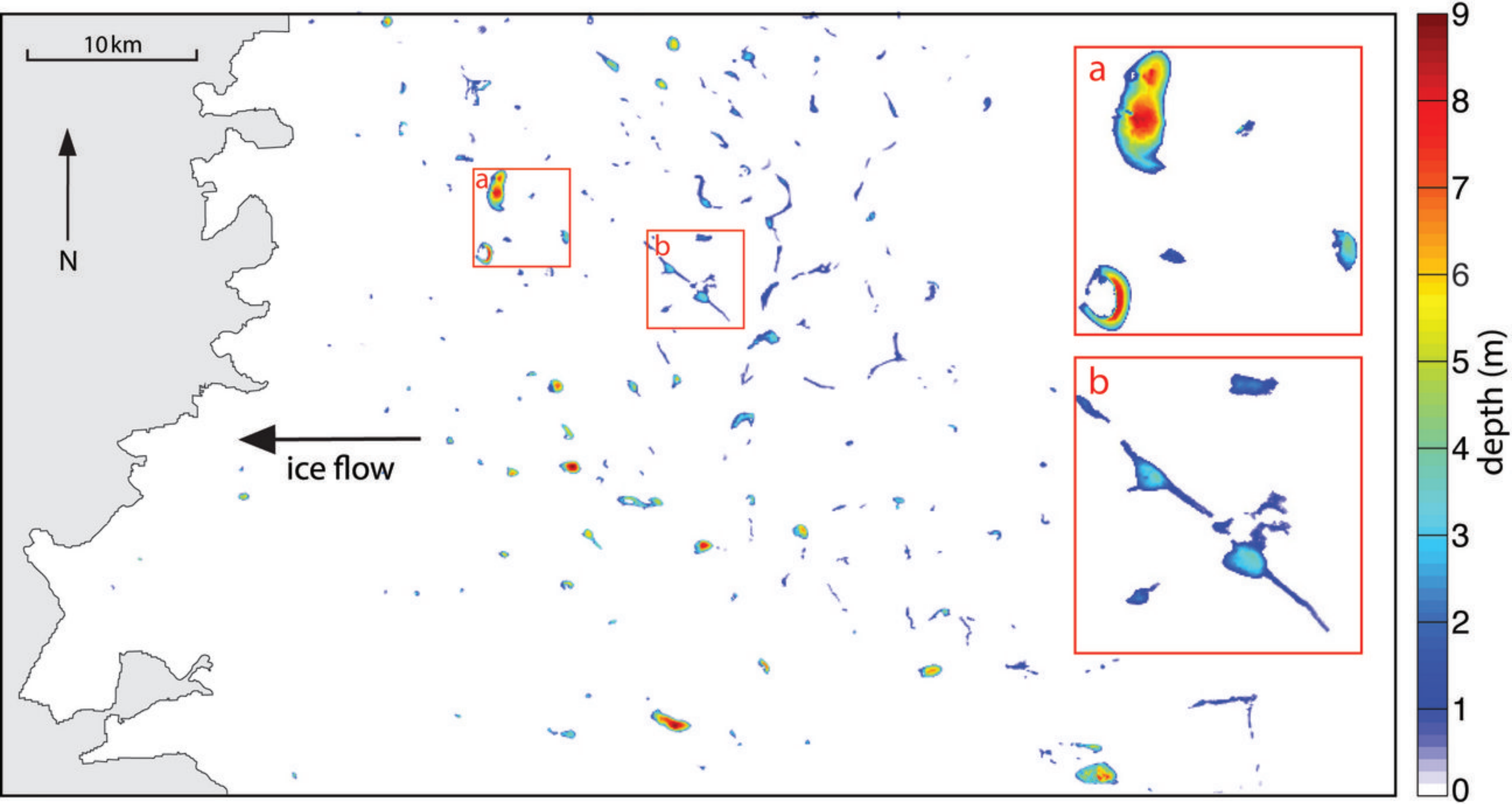
10 km
N
ice flow
a
b
depth (m)
0
1
2
3
4
5
6
7
8
9